Redox Mediation at 11-Mercaptoundecanoic Acid Self-Assembled Monolayers on Gold

Francesca Cecchet,[†] Massimo Marcaccio,[‡] Massimo Margotti,[‡] Francesco Paolucci,*[,‡] Stefania Rapino,[‡] and Petra Rudolf[§]

Laboratoire Interdisciplinaire de Spectroscopie Electronique, Facultés Universitaires Notre-Dame de la Paix, 61 rue de Bruxelles, B-5000 Namur, Belgium, Department of Chemistry "G. Ciamician" and INSTM, University of Bologna, via F. Selmi 2, I-40126 Bologna, Italy, and Materials Science Centre, Rijksuniversiteit Groningen, Nijenborgh 4, 9747AG Groningen, The Netherlands

Received: August 3, 2005; In Final Form: December 9, 2005

Cyclic voltammetry (CV), electrochemical impedance spectroscopy (EIS), and digital simulation techniques were used to investigate quantitatively the mechanism of electron transfer (ET) through densely packed and well-ordered self-assembled monolayers (SAMs) of 11-mercaptoundecanoic acid on gold, either pristine or modified by physically adsorbed glucose oxidase (GOx). In the presence of ferrocenylmethanol (FcMeOH) as a redox mediator, ET kinetics involving either solution-phase hydrophilic redox probes such as $[Fe(CN)_6]^{3-/4-}$ or surface-immobilized GOx is greatly accelerated: $[Fe(CN)_6]^{3-/4-}$ undergoes diffusion-controlled ET, while the enzymatic electrochemical conversion of glucose to gluconolactone is efficiently sustained by FcMeOH. Analysis of the results, also including the digital simulation of CV and EIS data, showed the prevalence of an ET mechanism according to the so-called *membrane model* that comprises the permeation of the redox mediator within the SAM and the intermolecular ET to the redox probe located outside the monolayer. The analysis of the catalytic current generated at the GOx/SAM electrode in the presence of glucose and FcMeOH allowed the high surface protein coverage suggested by X-ray photoelectron spectroscopy (XPS) measurements to be confirmed.

Introduction

Self-assembled monolayers (SAMs) of alkanethiols on gold, silver, and mercury have received enormous interest due to their reproducibility and the possibility to create a wide range of films with well-defined composition, thickness, and three-dimensional structure and an almost unlimited variety of surfaces via the incorporation of different functional groups at the end of the alkyl chains.[1−4] Long-chain ($n \geq 10$) alkanethiols form stable, close-packed, and well-ordered SAMs on gold electrodes that usually display a very low fraction of defects, are strongly resistant to ion penetration, and may therefore act as effective barriers to electron transfer (ET) processes involving solution-phase species.[5−8] They suppress background currents, control adsorption, reduce double-layer capacitance, inhibit corrosion, and enable a better control of electrode processes. The use of SAMs has greatly contributed to our knowledge of ET between a metal electrode and redox molecules, either adsorbed or in solution,[9,10] a problem that was approached by many different experimental techniques including photochemical, electrochemical, scanning probe microscopy, and temperature jump techniques.[1−4,11] ET to/from adsorbed redox species or hydrophilic homogeneous redox probes through nondefective SAMs does occur via nonresonant through-bond tunneling; that is, the rate decreases exponentially with the chain length, with decay constants ranging from 0.8−1.5 $Å^{-1}$ for saturated chains to 0.2−0.6 $Å^{-1}$ for unsaturated ones.[12] Short-chain alkanethiols, on the other hand, form relatively more disordered and therefore less blocking SAMs, they usually allow faster ET processes, and are preferred in the preparation for instance of bioelectrochemical devices where a good transduction of the biochemical signal is desired.[13−15] Short-chain SAMs however present some drawbacks with respect to their long-chain counterparts, namely, (i) a higher double-layer capacitance, that makes the signal-to-background ratio less favorable, (ii) a lower discrimination ability toward potential interferents, and (iii) lower reproducibility and robustness of the devices. The use of long-chain SAMs coupled with a suitable redox mediator, that is, a solution-phase species capable of undergoing fast ET processes in the presence of the blocking film, has been proposed for the electrochemical activation of enzymes and the construction of reliable electrochemical biosensors: neutral, hydrophobic redox species such as quinones, tetrathiafulvalene, and ferrocenyl derivatives have been widely investigated in such a context for their ability to undergo relatively fast ET at monolayer- and bilayer-modified electrodes.[16−18] In addition to tunneling, two alternative mechanisms for ET at SAM-modified electrodes are allowed for such species: (i) permeation of the redox probe through the monolayer (*membrane model*)[16−18] and, in more defective films, (ii) diffusion to pinholes and other defect sites and subsequent reaction at the bare electrode surface (*pinhole model*).[19]

Herein, we report on the study of the redox-mediated ET mechanism at a long-chain alkanethiol SAM involving either a solution-phase redox probe, $[Fe(CN)_6]^{3-/4-}$, or glucose oxidase (GOx) physically adsorbed at the SAM surface, using ferrocenylmethanol (FcMeOH) as a redox mediator. Stable and compact films of 11-mercaptoundecanoic acid (11-MUA) on gold were used in order to keep the fraction of pinholes and structural defects in the films as low as possible and have thus better insight into the kinetics of the mediated ET process. It is

* Corresponding author. E-mail: Francesco.Paolucci@unibo.it.
[†] Facultés Universitaires Notre-Dame de la Paix.
[‡] University of Bologna.
[§] Rijksuniversiteit Groningen.

10.1021/jp054290n CCC: $33.50
Published on Web 01/14/2006

well-known[1,9,10,20−22] in fact that alkanethiols with 9−12 methylene units optimize the balance between van der Waals interchain interactions and entropy loss due to ordering. Furthermore, the carboxylic end group is among the most versatile and used terminations for the subsequent functionalization of SAMs.[1−4,13−15]

The films, either pristine or functionalized by GOx, were investigated by X-ray photoelectron spectroscopy (XPS), cyclic voltammetry (CV), and electrochemical impedance spectroscopy (EIS). These techniques, widely used in the study of SAMs, allow one to evaluate the compactness of films, to measure the size (i.e., micropores vs macropores) and number of defects in the monolayer, to estimate the average thickness of the film via the evaluation of the double-layer capacitance of the modified electrode,[23,24] and to investigate the kinetics of ET processes at SAMs.[1−11]

Experimental Methods

Materials. 11-Mercaptoundecanoic acid (95%, Aldrich), glucose oxidase (GOx) (EC 1.1.3.4. from Aspergillus Niger, Fluka), KCl (pro analysi from Merck), ferrocenylmethanol (Strem Chemicals), $K_4[Fe(CN)_6]$ and $K_3[Fe(CN)_6]$ (Aldrich), glucose (Sigma), chloroform (HPLC grade, Acros), and phosphate buffer (pH 7, from Merck) were used as received. Millipore water was used in the preparation of solution, and all other materials were reagent grade chemicals.

Preparation of Monolayers. The substrates were evaporated gold films supported on Si(111) wafers (IMEC, Belgium). They were cleaned in an ozone discharge for 15 min, followed by sonication in ethanol for 20 min immediately before being employed. Carboxylic acid-terminated SAMs were prepared by immersion of the gold substrates in a 1 mM chloroform solution of 11-MUA for 21 h. The samples were rinsed in chloroform and dried under argon before introduction into ultrahigh vacuum for characterization by X-ray photoelectron spectroscopy (XPS).[20,21]

Protein Adsorption. Glucose oxidase was diluted in a phosphate buffered aqueous solution (pH 7) to a concentration of 1 mg/12 mL. Self-assembled monolayers of 11-MUA were immersed in the protein solution for 24 h and then abundantly rinsed and sonicated in the pure buffer solution before analysis by X-ray photoelectron spectroscopy, cyclic voltammetry, and impedance spectroscopy.

X-ray Photoelectron Spectroscopy (XPS) Analysis. High-resolution XPS measurements were performed using an SSX-100 (Surface Science Instruments) photoelectron spectrometer with a monochromatic Al Kα X-ray source ($h\nu = 1486.6$ eV). The energy resolution was set to 0.92 eV to minimize data acquisition time, and the photoelectron take-off angle (TOA) was 90°. All binding energies were referenced to the Au $f_{7/2}$ core level (Moulder, J. F.; Stickle, W. F.; Sobol, P. E.; Bomben, K. D. *Handbook of Photoelectron Spectroscopy*; Perkin-Elmer Corporation, Physical Electronics Division: Eden Prairie, MN, 1992). The base pressure in the spectrometer was in the low 10^{-10} Torr range. Spectral analysis included a linear background subtraction and peak separation using mixed Gaussian−Lorentzian functions, in a least-squares curve-fitting program (Winspec) developed in the LISE laboratory of the University of Namur.

Electrochemical Instrumentation and Measurements. The electrochemical experiments were performed in either unbuffered 0.1 M KCl or phosphate buffered (pH 7) aqueous solutions, using a two-compartment electrochemical cell also fitted with a saturated calomel electrode (SCE) and a platinum spiral as counter electrode. CV and EIS experiments (in the frequency range from 100 kHz to 0.05 Hz) were carried out with an Autolab model PGSTAT 30 (ECO CHEMIE) instrument. The CV simulations were carried out by the DigiSim 3.0 software by Bioanalytical Systems Inc. All of the simulation parameters that were known from the literature are properly referenced. All of the other parameters (except those directly obtained from experiment, for example, $E°$'s) were instead obtained by fitting procedures. All of the fitting parameters were chosen so as to obtain a visual best fit over a 10-fold range of scan rates.

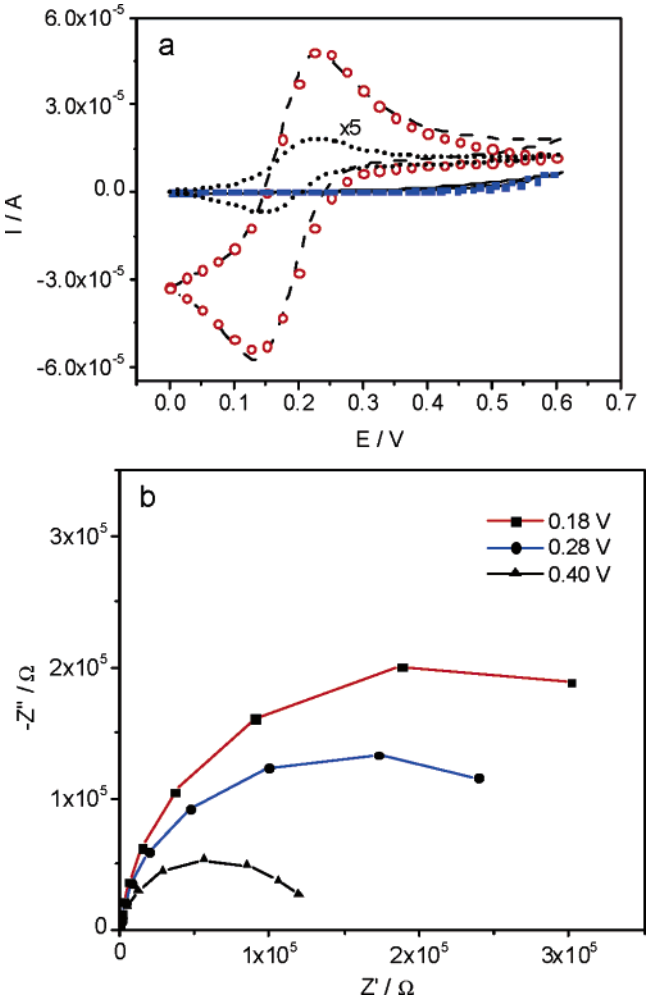

Figure 1. (a) CV curves on an 11-MUA-modified gold electrode (area 1 cm^2): (full line) an aqueous solution of 2.0 mM $[Fe(CN)_6]^{3-/4-}$ and 0.1 M KCl; (dashed line) after the addition of FcMeOH (0.1 mM); (dotted line) 0.1 mM FcMeOH, 0.1 M KCl; (blue squares) digital simulation obtained according to the tunneling equation ($k_{SAM} = k_{Au} \times e^{-\beta n}$, where $k_{Au} = 0.031$ cm s^{-1} and $\beta = 0.93$, the electron transfer coefficient, α, was kept constant at 0.5), $E°([Fe(CN)_6]^{3-/4-}) = 0.18$ V; (red circles) digital simulation obtained according to Scheme 2 (eqs 1−4) [$K_n = 0.025$, $K_o = 34$, $K_{redox} = 1$, $k° = 0.14$ cm s^{-1}, $\alpha = 0.5$, $E°(FcMeOH)^{+/0} = 0.18$ V]. Scan rate: 0.02 V/s. (b) Nyquist plots recorded on an 11-MUA-modified gold electrode in an aqueous solution of 1 mM $[Fe(CN)_6]^{3-/4-}$ and 0.1 M KCl at 0.18 V (■), 0.28 V (●), and 0.40 V (▲).

Results and Discussion

Figure 1a (full line) shows the CV curve obtained at the 11-UMA/gold electrode in a 2 mM $[Fe(CN)_6]^{3-/4-}$ aqueous solution (i.e., a 2 mM solution of both $[Fe(CN)_6]^{3-}$ and $[Fe(CN)_6]^{4-}$). The mostly capacitive and low-intensity curve was stable and highly reproducible; the absence of any sigmoidal behavior,

SCHEME 1: Randles Equivalent Circuit Describing the Electrical Response of the Electrochemical Interface[a]

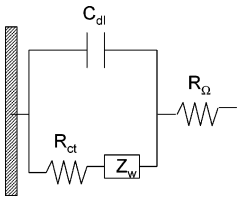

[a] In the circuit, R_Ω represents the solution resistance, C_{dl}, the double-layer capacitance, R_{ct}, the charge transfer resistance (related to the exchange current, i_0, and standard rate constant), and Z_W, the Warburg element, describing the time (frequency) dependence of mass transport.

indicative of kinetically active pinhole-like defects,[1,19] or peak-shaped morphology, associated with a large contribution from defect sites or permeation (vide infra),[24] testify for the highly blocking character of the SAM. The digital simulation of the CV curve calculated according to the tunneling equation, that is, assuming that the heterogeneous ET rate constant is $k_{SAM} = k_{Au} \times e^{-\beta n}$, where $k_{Au} = 0.031$ cm s^{-1} (see ref 24) and using an electronic tunneling factor per methylene unit of $\beta = 0.93$,[1−3,9−12] shown in Figure 1a (blue squares), is in fact in very good agreement with the experimental one.

The highly blocking character of the SAM was also assessed by performing an EIS analysis under the above conditions. In Figure 1b, the out-of-phase component of the impedance, $-Z''$, plotted versus the in-phase one, Z', with Z'' and Z' being parametric functions of the frequency (Nyquist plot), is shown as a function of potential.[26] The incomplete semicircles that rapidly shrink upon increasing overpotential are associated with the slow electron transfer kinetics experienced by the redox probe at the modified electrode. The spectrum obtained under open-circuit conditions was fitted according to the Randles equivalent circuit (Scheme 1), using the CNLS method described by Boukamp.[27] The evaluation of the standard heterogeneous ET rate constant is simplified by using the same concentrations for both members of the redox couple (i.e., equimolar $[Fe(CN)_6]^{3-}$ and $[Fe(CN)_6]^{4-}$). Under such conditions, the open-circuit potential, E_{oc}, coincides with $E^\circ_{[Fe(CN)_6]^{3-/4-}} = 0.18$ V, and the standard heterogeneous ET rate constant is related to R_{ct} by the following relationship: $k^\circ = (RT/n^2F^2AC_0)(1/R_{ct})$. From the value of R_{ct} measured at E_{oc}, an apparent standard rate constant value for the ET process of 1.1×10^{-6} cm s^{-1} was obtained, in very good agreement with the value obtained through the simulation of the CV curve (see above).

At the same time, the low value of C_{dl} obtained from the fitting (3.19 μF cm^{-2}) is also typical of electrodes covered by a well-formed SAM of COOH-terminated long-chain thiols.[1] Within the Helmholtz capacitor approximation of the double layer and assuming a dielectric constant of the organic layer of $\epsilon = 4$,[1] from the best-fit value for C_{dl}, an average thickness of the SAM amounts to $t = \epsilon\epsilon_0/C_{dl} = 12.5$ Å. Taking into account the length of the 11-MUA molecule (16.1 Å), this value for t indicates that 11-MUA forms a close-packed SAM with molecules tilted between 35 and 40° from the surface normal, in agreement with previous reports.[1,4] Notice that, in the fitting of the EIS spectra shown in Figure 1 (as of all those shown in this work), a *pure capacitive* behavior of the double layer was assumed; that is, no use of the constant-phase element (CPE) was made. The use of such an element in the Randles equivalent circuit is usually associated with nonideal behavior due to surface roughness and anomalous transport effects and, in particular, in the presence of collapsed sites and defects in SAMs.[24,28−31] Since a very good fitting of the EIS spectra was obtained in this case using the simple capacitive element C_{dl} (chi-square was typically in the range of 10^{-5}), the inference is that the 11-MUA SAMs are ideally blocking and their structural defects are immeasurable by electrochemical techniques.[24]

SCHEME 2: Mechanism of ET of FcMeOH at a SAM on Gold According to the Permeation Model (eqs 1−3) and FcMeOH-Mediated Reduction/Oxidation of $[Fe(CN)_6]^{3-/4-}$ (eqs 1−4)[a]

$$\mathrm{FcMeOH} \overset{K_n}{\rightleftharpoons} \mathrm{M} \quad (1)$$

$$\mathrm{M} \overset{k^\circ}{\rightleftharpoons} \mathrm{M^+ + e} \quad (2)$$

$$\mathrm{M^+} \overset{K_o}{\rightleftharpoons} \mathrm{FcMeOH^+} \quad (3)$$

$$[Fe^{II}(CN)_6]^{4-} + \mathrm{FcMeOH^+} \overset{K_{redox}}{\rightleftharpoons} [Fe^{III}(CN)_6]^{3-} + \mathrm{FcMeOH} \quad (4)$$

[a] M and M^+ in the scheme denote the redox mediator (=FcMeOH) within the membrane. K_n and K_o are the equilibrium constants relative to mediator partitioning between solution and monolayer, in the neutral and oxidized state, respectively, k° is the standard rate constant of FcMeOH on gold (0.14 cm s^{-1}),[16,17] and K_{redox} is the equilibrium constant of the homogeneous redox process: $K_{redox} = \exp\{F/RT[E^\circ([Fe(CN)_6]^{3-/4-}) - E^\circ(\mathrm{FcMeOH^{+/0}})]\} \sim 1$.

The packing density of the alkane chains is not the only factor governing ion permeability and ET processes, since the nature of the terminal group is also expected to affect the ET kinetics. Both the potential drop across the monolayer and the concentration of a charged redox probe at the SAM surface may be in fact influenced by the terminal charge of functionalized SAMs.[1,32,33] As a matter of fact, a somewhat less blocking behavior was found when a different hydrophilic redox probe was used, namely, $[Ru(NH_3)_6]^{3+}$, as a likely consequence of the combination of (i) a higher standard ET rate constant with respect to $[Fe(CN)_6]^{3-/4-}$ and (ii) the positive charge of the redox probe. However, a very similar blocking behavior with $[Fe(CN)_6]^{3-/4-}$ to that observed in the case of the 11-MUA SAM was also found in the case of CH_3-terminated SAMs (C_{12}), thus suggesting that factor ii is relatively less important in determining the ET kinetics.

At variance with hydrophilic redox probes, hydrophobic ones, such as quinones, water-soluble ferrocene derivatives (such as FcMeOH and ferrocenedimethanol),[16−18,34−39] and menadione,[16−18] may undergo fast ET at highly blocking SAMs. The so-called *membrane model* was proposed for explaining such a behavior which assumes that the redox probe may *permeate* into the monolayer and approach the electrode surface. Permeation does not imply the existence of pinholes or other structural defects and may take place through well-oriented SAM domains, because of dynamic fluctuations in the SAM (in particular, COOH-terminated SAMs are *liquidlike*[1]), driven by the hydrophobicity of the redox probe. Such a mechanism was recently investigated by various electrochemical techniques, including CV and scanning electrochemical microscopy,[11,16,17,40] and a mathematical model has recently been proposed that comprises partitioning equilibria of the redox probe between solution and SAM and ET occurring (within the membrane) with identical kinetic parameters as compared to those at the bare electrode.[16,17] Such a mechanism is illustrated in Scheme 2 (eqs 1−3). The assumption that the electrochemical parameters are the same as those at the bare electrode may represent an oversimplification because ET does not occur in fact in the same medium (e.g., reorganization energies and viscosity are different),[16,17] and furthermore, the spatial distribution of reactant within the SAM

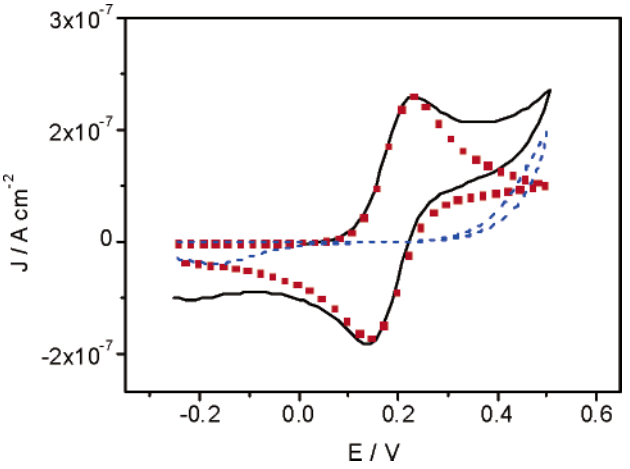

Figure 2. (full line) CV curve (normalized by the electrode area) of an aqueous solution of 0.05 mM FcMeOH and 0.1 M KCl on an 11-MUA-modified gold electrode (area 0.15 cm^2); (dashed blue line) digital simulation obtained according to the tunneling equation ($k_{SAM} = k_{Au} \times e^{-\beta n}$, where $k_{Au} = 0.14$ cm s^{-1}, $\beta = 0.93/CH_2$, $\alpha = 0.5$, and $E°(FcMeOH)^{+/0} = 0.18$ V); (red squares) digital simulation obtained according to Scheme 2 (eqs 1−3) [$K_n = 0.025$, $K_o = 34$, $k° = 0.14$ cm s^{-1}, and $E°(FcMeOH)^{+/0} = 0.18$ V]. Scan rate: 0.02 V/s.

should also be taken into account reflecting the spatial extent over which most of the ET occurs.[41] Figure 2 (full line) shows the CV curve measured for a diluted (0.05 mM) aqueous solution of FcMeOH at the 11-MUA SAM.

The curve displays the typical shape expected for diffusion-controlled reversible redox processes. Outside the region of CV peaks, the current increases above the expected levels for diffusion-controlled ET processes and a low broad peak is also observed with $E_p \approx -0.22$ V. Such features, that cannot be ascribed to Au oxidation/reduction, as observed at nonideally blocked electrodes,[42] would instead suggest that, along with permeation, tunneling may also contribute, although to a little extent, to ET. Not unexpectedly, such features were in fact much less evident in the CV curves obtained at relatively higher FcMeOH concentrations (Figure 1a, dotted line).

On the basis of the model depicted in Scheme 2, formally identical to a CEC (Chemical Electrochemical Chemical) mechanism,[16,17] the simulated curve shown in Figure 2 (red squares) was obtained and found to be in rather good agreement with the experimental one. As expected, the simulation failed to reproduce the additional features, observed in the CV curve closer to the potential window limits, that were attributed to tunneling (see simulated curve in Figure 2, dashed line).

The fast ET kinetics typical of FcMeOH and related species at SAMs make them efficient redox mediators to/from hydrophilic species free in solution or immobilized at the SAM outer surface. The addition of small amounts of FcMeOH to $[Fe(CN)_6]^{3-/4-}$ aqueous solutions results in fact in the dramatic changes shown in Figure 1a (dashed line), where the reversible CV pattern displays now the typical features of diffusion-controlled curves. Permeating into the monolayer, and being oxidized at the electrode, FcMeOH would then promote the oxidation of $[Fe(CN)_6]^{4-}$ to $[Fe(CN)_6]^{3-}$, thus effectively shuttling electrons through the monolayer. Notice however that the CV curve relative to $[Fe(CN)_6]^{3-/4-}$ shown in Figure 1 (dashed line) differs at a fundamental level from that relative to the single mediator, measured in the absence of $[Fe(CN)_6]^{3-/4-}$ and also shown, for the sake of comparison, in Figure 1a (dotted line). While in the latter curve no current is observed at the starting potential (0 V) (oxidation of FcMeOH is in fact the only expected process), that measured in the presence of

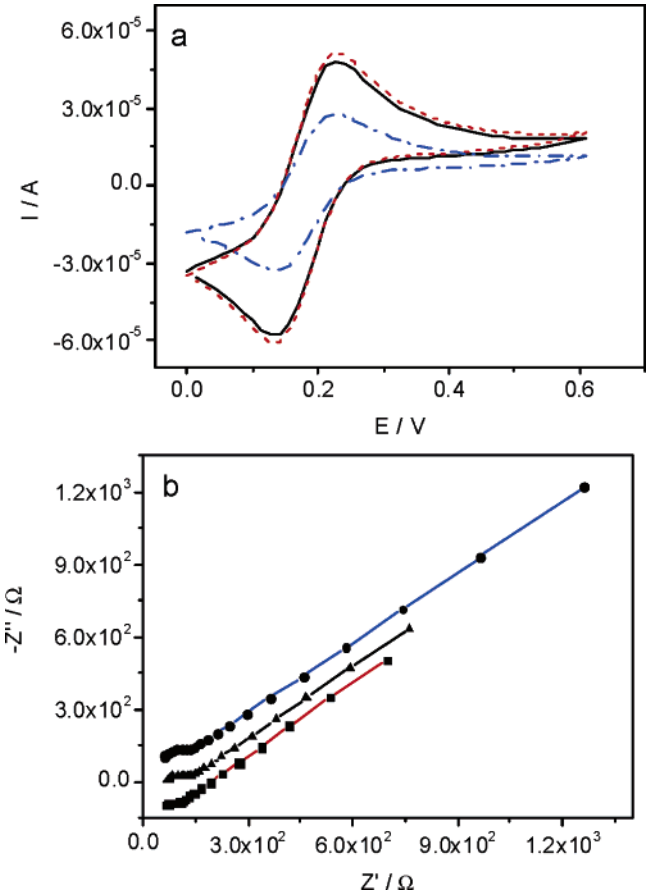

Figure 3. CV curves and Nyquist plots recorded on an 11-MUA-modified gold electrode (area 1 cm^2) illustrating the effects of changes of substrate and/or redox mediator concentration. (a) CV curves of an aqueous solution of (full line) 2 mM $[Fe(CN)_6]^{3-/4-}$, 0.1 mM FcMeOH, and 0.1 M KCl; (dashed red line) 2 mM $[Fe(CN)_6]^{3-/4-}$, 0.2 mM FcMeOH, and 0.1 M KCl; (dash−dot blue line) 1 mM $[Fe(CN)_6]^{3-/4-}$, 0.1 mM FcMeOH, and 0.1 M KCl. Scan rate: 0.02 V/s. (b) Nyquist plots under the same conditions as those in part a: (▲) 2 mM $[Fe(CN)_6]^{3-/4-}$, 0.1 mM FcMeOH, and 0.1 M KCl; (■) 2 mM $[Fe(CN)_6]^{3-/4-}$, 0.2 mM FcMeOH, and 0.1 M KCl; (●) 1 mM $[Fe(CN)_6]^{3-/4-}$, 0.1 mM FcMeOH, and 0.1 M KCl. For better readibility, the spectra were shifted vertically by ±100 Ω with respect to one another.

$[Fe(CN)_6]^{3-/4-}$ displays a significant cathodic current at the starting potential. This implies that, at such a potential, $[Fe(CN)_6]^{4-}$ is oxidized through the mediation of $FcMeOH^+$, which must therefore necessarily be already present in solution, with its production at the electrode being thermodynamically unfavored at such potentials. The inference is that the homogeneous redox process between $[Fe(CN)_6]^{3-}$, $[Fe(CN)_6]^{4-}$, and FcMeOH (eq 4 of Scheme 2) can reach the equilibrium in the time scale of the voltammetric experiments.

The whole mediated ET mechanism is summarized in Scheme 2 (eqs 1−4). The equilibrium constant of the homogeneous redox process between the two redox couples is expectedly ∼1 due to the accidental near coincidence of their $E°$ values. The simulated CV curve, calculated according to such a mechanism, is shown in Figure 1a (red circles) and is in very good agreement with the experimental one. The CV peak heights are proportional to the $[Fe(CN)_6]^{3-/4-}$ concentration (compare in Figure 3a, full and dash−dot lines), thus highlighting the great efficiency of $FcMeOH^{0/+}$ to mediate ET to/from $[Fe(CN)_6]^{3-/4-}$. Such a process is in fact under diffusion control and is not kinetically limited by the availability of the redox mediator in the diffusion layer, as also shown by the negligible current increase observed

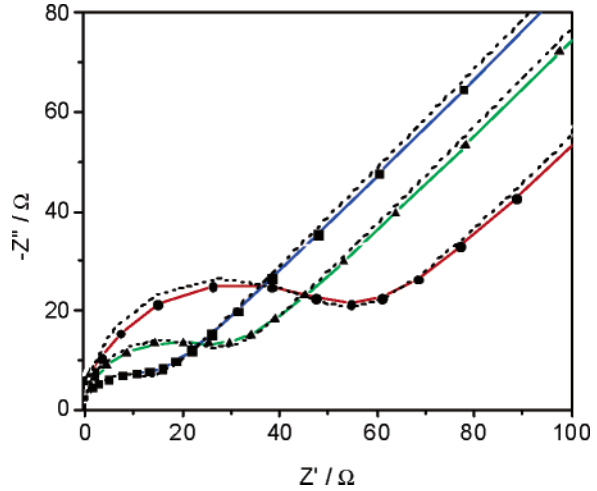

Figure 4. Nyquist plots recorded on an 11-MUA-modified gold electrode (area 1 cm^2) illustrating the effects of changes of redox mediator concentration. For a better readibility, the solution ohmic resistance, R_Ω, was subtracted from the real part of the impedance data. (●) 2 mM $[Fe(CN)_6]^{3-/4-}$, 0.1 mM FcMeOH, and 0.1 M KCl; (▲) 2 mM $[Fe(CN)_6]^{3-/4-}$, 0.2 mM FcMeOH, and 0.1 M KCl; (■) 2 mM $[Fe(CN)_6]^{3-/4-}$, 0.4 mM FcMeOH, and 0.1 M KCl. Dashed lines: fitting of EIS spectra assuming the Randles equivalent circuit (Scheme 1).

TABLE 1: 11-MUA SAM on Gold—Electrical Parameters of the Randles Equivalent Circuit Evaluated by Fitting Procedures from EIS Data Shown in Figure 4[a]

[FcMeOH] (mM)	$[Fe(CN)_6]^{3-/4-}$ (mM)	R_Ω (Ω)	R_{ct} (Ω)	C_{dl} (μF cm^{-2})	$Y_0 \times 10^{-2}$ (Ω^{-1} $s^{1/2}$)
0.1	1	60.2	52.9	3.3	0.11
0.1	2	71.2	47.4	3.2	0.20
0.2	2	68.2	24.3	3.0	0.21
0.4	2	57.1	11.96	2.9	0.23

[a] The Warburg impedance, Z_W, is related to Y_0 and frequency by the relationship $Z_W = 1/Y_0\sqrt{i\omega}$,[26] where $i = \sqrt{-1}$ and ω is the angular frequency ($=2\pi f$).

upon doubling the FcMeOH concentration (compare in Figure 3a, full and dashed lines).

The mediation model depicted in Scheme 2 was further validated by EIS, which also provided a more quantitative description of it with respect to voltammetry. Figure 3b compares the impedance spectra measured at E_{OC} (=0.18 V) obtained in the presence of various concentrations of $[Fe(CN)_6]^{3-/4-}$ and FcMeOH (i.e., under the same conditions as those in Figure 3a).

In all cases, charge transfer and double-layer charging dominate the interface response at medium-high frequencies (semicircles), while the 45° straight line observed in the low-frequency range (Warburg line) shows the prevalence of mass transport in longer time scales.[26] Notice that, in the EIS spectra measured in the absence of FcMeOH (Figure 1b), no such Warburg-like behavior was observed at frequencies as low as 0.05 Hz. The effect of FcMeOH concentration on the rate of the charge transfer process is better evidenced in Figure 4.

The electrical response of the interface as shown in Figures 3b and 4 was quantitatively described in terms of the Randles equivalent circuit (Scheme 1) whose electrical parameters were evaluated by fitting procedures (see dashed lines in Figure 4), using the CNLS method described by Boukamp.[27] The best-fit values of the various elements in the circuit of Scheme 1, measured at E_{oc}, are reported in Table 1.

Notice that the R_{ct} values are ~3 orders of magnitude lower than that measured for $[Fe(CN)_6]^{3-/4-}$ in the absence of FcMeOH (60.6 Kohm). Moreover, a doubling of the $[Fe(CN)_6]^{3-/4-}$ concentration halved the Warburg element, Z_W, while each doubling of the FcMeOH concentration halved the R_{ct} value (compare such effects on the straight line lengths in Figure 3b and semicircle diameters in Figure 4). Given the inverse proportionality dependence of R_{ct} (see above) and Z_W [$Z_W = 1/Y_0\sqrt{i\omega}$, where $1/Y_0 = (RT/F^2A\sqrt{2}) \times ((1/D_o^{1/2}C_o^*) + (1/D_r^{1/2}C_r^*))$] on the concentration of the relevant redox couple, the above concentration effects substantiate the model depicted in Scheme 2, that is, the hypothesis that $[Fe(CN)_6]^{3-/4-}$ may undergo fast (diffusion-controlled) ET at the 11-MUA SAM via the efficient redox mediation of $FcMeOH^{0/+}$. From the R_{ct} values in Table 1, the apparent standard ET rate constant for FcMeOH was calculated to be 0.056 cm s^{-1}: despite the presence of the compact monolayer, such a value is only half the value measured at bare gold.

Water-soluble substituted ferrocenes, and in particular ferrocenylmethanol, ferrocenedimethanol, and ferrocene carboxylate, have often been used to promote the redox-mediated bioelectrocatalytic process in enzymatic amperometric biosensors where the enzyme is either homogeneously dispersed in solution[13−18,34−39] or entrapped at the SAM-modified electrode surface.[13−18,38,39,44,45] Effects on the dynamics of mediated ET are in particular expected in the case of the immobilized enzymes mainly because of changes in the partitioning of the redox mediator at the modified SAM boundary. Such effects were then investigated by the combined use of CV and EIS.

GOx-modified SAMs were obtained by immersion in the protein solution in a phosphate buffer (pH 7) for 24 h, followed by abundant rinsing and sonication in the pure buffer solution (see the Experimental Section). The simple procedure adopted herein for GOx immobilization did not bring about the same long-term stability as usually observed in the case of covalent binding of the protein (e.g., by 1-(3-dimethylaminopropyl)-3-ethylcarbodiimide) on COOH-terminated SAMs.[13,18,44,46] The functionalized surfaces were however stable enough to allow their characterization by X-ray photoelectron spectroscopy (XPS) as well as by electrochemistry. While the search for long-term stability was outside the scope of the present work, the reason the protein may also adsorb strongly onto the 11-MUA surface in the absence of any chemical activation of the terminal groups still remains unclear. In fact, both the protein and the SAM surface are expected to carry, at pH 7, a net negative charge and repulsive forces should therefore prevent adsorption. The isoelectric point of the native protein is in fact 4.2, while values ranging between 4.5 and 5.6 have been reported for the pK_a of the SAM terminal COOH groups (known to have higher pK_a's than those for the same molecules in solution).[47,48] It may however be expected that the magnitude of such repulsive forces be partially compensated for by ion binding between the COO^- groups and the counterions in the electrolyte. This might in turn allow for the protein to approach the SAM surface and become trapped to it by the formation of multiple H-bonds. The role of counterions at charged interfaces in important processes such as colloidal suspension, biomineralization, and ionic transport though membranes has already been outlined, and also known is the relevance of the ionic environment in SAM properties.[47]

Figure 5a shows the carbon 1s core level photoemission spectrum for a monolayer of 11-MUA.

As already discussed in a previous work,[4,20,21] the analysis of the carbon 1s core level region recorded for the monolayer provides the identification of a main peak centered at 284.8 eV which is assigned to the aliphatic carbons of the alkyl chains, while the last feature at 289.6 eV corresponds to the carboxylic

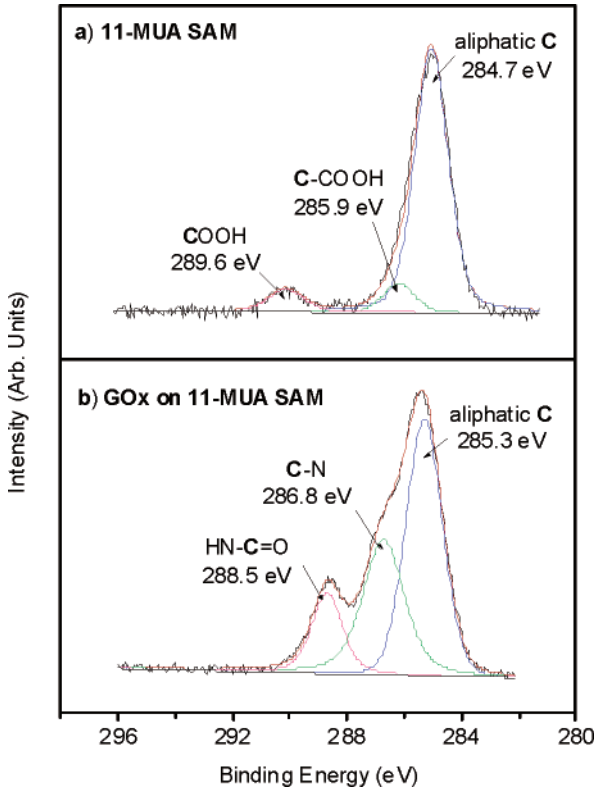

Figure 5. Photoemission spectra and fit of the C 1s core level region for (a) a film of 11-MUA and (b) a film of 11-MUA functionalized with GOx.

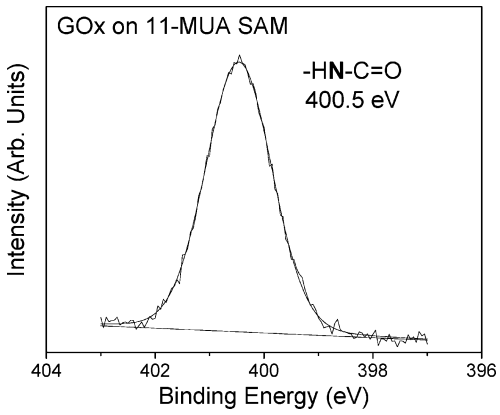

Figure 6. Photoemission spectra of the N 1s core level region for a film of 11-MUA functionalized with GOx.

carbon atom of the acid group. A remarkable change is shown in the C 1s core level spectrum recorded for the 11-MUA self-assembled monolayer modified with GOx protein (Figure 5b). The main peak at 285.3 eV is still assigned to pure aliphatic carbon atoms from the 11-MUA SAM and from the protein, while the higher binding energy peaks are the signals characteristic of peptide functions of proteins: the peak at 286.8 eV is attributed to C−N peptide bonds, while the last peak at 288.5 eV is due to C═O bonds of peptide moieties of protein.[49] The carboxylic carbon signal, coming from the SAM, is here not detectable anymore because of the strong intensity of the C═O protein bond signal, showing the high coverage of proteins onto the SAM.

Figure 6 shows the N 1s core level region recorded for the 11-MUA SAM functionalized with GOx: the experimental feature is fitted by one component centered at 400.5 eV, which is the typical binding energy of the amide nitrogen atoms,[50] coming from the peptide functions of protein.

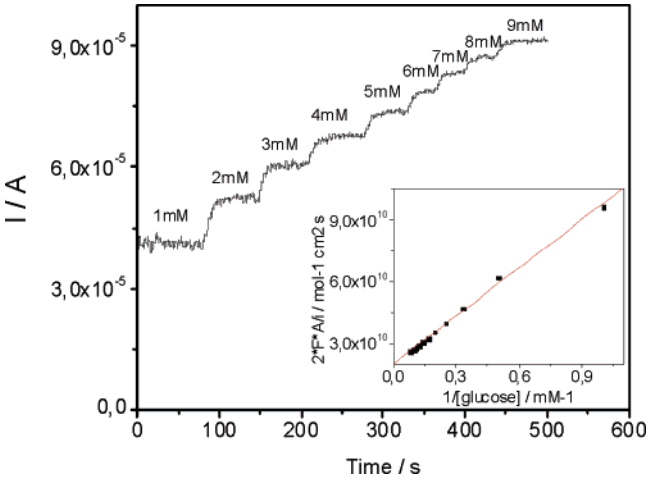

Figure 7. Amperometric response of the GOx/11-MUA-modified gold electrode (area 1 cm^2) in the presence of FcMeOH (1 mM) upon subsequent additions of β-D-glucose. Conditions: deareated phosphate buffered (pH 7) aqueous solution; potential of 0.2 V, $T = 25$ °C. Inset: Lineweaver−Burk plot of the catalytic currents shown in the main plot.

An estimation of the surface coverage from the attenuation of the gold signal in the XPS data, following the protein adsorption, was not attempted because of the uncertainty of the inelastic mean free path values for proteins. Nevertheless, since the analysis depth of XPS is at most 10 nm in normal emission, the fact that the gold signal is still observed after protein adsorption suggests that the average film thickness is lower than 10 nm. GOx is a globular protein made up of two identical subunits, each measuring 60 Å × 52 Å × 37 Å, linked by disulfide bonds.[51] The corresponding dimer dimensions are 70 Å × 55 Å × 80 Å. As discussed in a previous work,[4] the average thickness for the 11-MUA SAM has been estimated to be 12.5 ± 0.6 Å. We can therefore deduce that the average thickness of the film is in agreement with a single layer of GOx proteins adsorbed to the SAM.

The 11-MUA SAM/Au electrode carrying the monolayer of GOx was transferred into a deareated phosphate buffered (pH 7) aqueous solution. The electrode potential was held at 0.2 V, and the anodic current (corresponding to oxidation of FcMeOH) was monitored while adding subsequent amounts of glucose. After each addition, an anodic current step occurred that reached its final, stationary value within ∼20 s (Figure 7), thus suggesting mass transport control onto the electrocatalytic conversion of β-D-glucose to δ-D-gluconolactone, that is described by the ping-pong mechanism of oxidoreductases illustrated in Scheme 3.[34] In agreement with such a behavior, also described in similar bioelectrocatalytic systems,[13] the Warburg impedance as measured by EIS (vide infra) was, in the case of the GOx-modified SAM, 1 order of magnitude higher than that measured for the $[Fe(CN)_6]^{3-/4-}$/FcMeOH system described above (compare Tables 1 and 2). The limiting current increment was obtained for [glucose] ≥ ∼12 mM. The catalytic response under steady-state conditions was stable for several minutes, thus highlighting that desorption of protein over the time scale of voltammetric (and EIS) was not significant.

From the analysis of current increments as a function of glucose concentration, the apparent Michaelis−Menten constant $K_M' = 4.3$ mM was estimated. As expected, no catalytic response was obtained in the absence of FcMeOH because of the lack of direct electric contact between the flavin active site of GOx and the electrode surface.

Figure 8a compares the CV curves obtained at the stationary SAM-modified gold electrode after GOx immobilization in the

SCHEME 3: Mechanism of FcMeOH-Mediated Enzymatic Amperometric Oxidation of Glucose[a]

$$S + E_{ox} \underset{k_{-1}}{\overset{k_1}{\rightleftharpoons}} SE_{ox} \xrightarrow{k_2} P + E_{red} \quad (5)$$

$$FcMeOH^+ + E_{red} \xrightarrow{k_3} FcMeOH + E_{red/ox} \quad (6)$$

$$FcMeOH^+ + E_{red/ox} \xrightarrow{k_4} FcMeOH + E_{ox} \quad (7)$$

$$FcMeOH^+ + e \underset{}{\overset{k_{app}}{\rightleftharpoons}} FcMeOH \quad (8)$$

[a] S and P represent β-D-glucose and δ-D-gluconolactone, respectively. E_{ox}, SE_{ox}, E_{red}, and $E_{red/ox}$ are the oxidized form of GOx (GOx-FAD), the complex of GOx-FAD and substrate, the reduced form of GOx (GOx-$FADH_2$), and the semiquinoid form of GOx (GOx-$FADH^{\bullet}$), respectively. The rate constants k_1, k_{-1}, k_2, k_3, and k_4 are related to the Michaelis−Menten constants for the substrate, K_S [$=(k_{-1} + k_2)/k_1$], and for the mediator, K_M [$=k_2(k_3 + k_4)/k_3k_4$], respectively. k_2 is the turnover number of GOx, and k_{app} is the apparent heterogeneous rate constant of FcMeOH at the GOx/SAM/gold electrode.

TABLE 2: Glucose Oxidase-Modified 11-MUA SAM on Gold−Electrical Parameters of the Randles Equivalent Circuit Evaluated by Fitting Procedures from EIS Data Shown in Figure 8b[a]

	R_Ω (Ω)	C_{dl} (μF cm^{-2})	R_{ct} (Ω)	$Y_0 \times 10^{-3}$ (Ω^{-1} s$^{1/2}$)	B (s$^{1/2}$)
FcMeOH (0.1 mM)	66.8	1.5	93.4	0.32	
FcMeOH (0.1 mM) + glucose (12 mM)	67.5	1.9	145.6	0.30	0.52

[a] The Warburg impedance, Z_W, is related to Y_0 and frequency by the relationship $Z_W = 1/Y_0\sqrt{i\omega}$,[26] where $i = \sqrt{-1}$ and ω is the angular frequency ($=2\pi f$), or to Y_0 and B according to eq 9.

presence of FcMeOH (1 mM) and either in the absence (full line) or in the presence (dashed line) of a large concentration of β-D-glucose (9 mM). In Figure 8b, the impedance plots measured under the same conditions are shown. In the absence of glucose (squares), Randles-type behavior, similar to that shown in Figure 3b, was observed. The 45° straight line at low frequencies (Warburg line) is associated to semi-infinite diffusion of FcMeOH. In agreement with the steady-state CV behavior shown in Figure 8a, such a straight line is replaced, in the presence of glucose (dots), by a semicircle as usually observed in the case of finite diffusion.[52,53] The EIS spectra of Figure 8b were fitted according to the Randles equivalent circuit shown in Scheme 1, where the mass transport element was either a Warburg element for semi-infinite diffusion (see table captions) or the hyperbolic tangent element (eq 9)

$$Z_W = 1/Y_0\sqrt{i\omega}\,\tanh(B\sqrt{i\omega}) \quad (9)$$

In such an element, usually adopted in the case of finite diffusion,[52,53] the parameter B is related to the thickness of the Nernstian diffusion layer, δ_N, and to the diffusion coefficient by the relationship $\delta_N = B \times D^{1/2}$. The significantly lower C_{dl} value obtained in the case of protein-modified SAM with respect to pristine 11-MUA SAM (~1.5 vs ~3 μF cm^{-2}, compare Tables 1 and 2) is associated to the high protein coverage also evidenced by XPS. Analogously, R_{ct} increases in the presence of the protein layer as a likely effect on partitioning of the redox mediator between solution and membrane. Interestingly, both C_{dl} and R_{ct} change (increase) upon addition of glucose (vide Table 2) as a probable consequence of conformational changes of the protein layer following either the enzyme/substrate binding event or the enzymatic production of gluconic acid (with

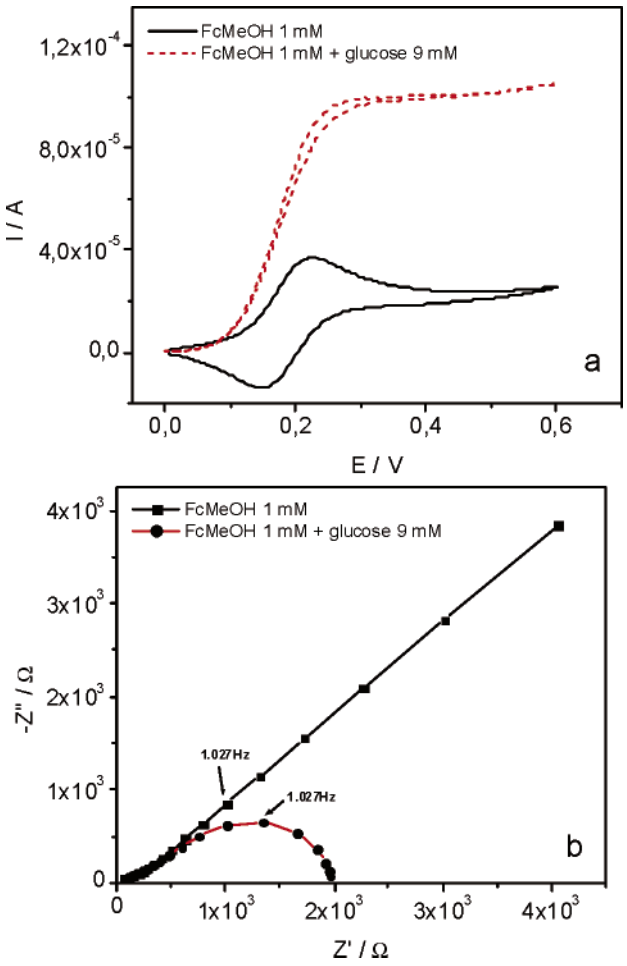

Figure 8. (a) CV curves recorded at $\upsilon = 0.02$ /s and (b) EIS spectra obtained at $E = 0.18$ V on an 11-MUA-modified gold electrode (area 1 cm^2) immersed in a 1 mM FcMeOH (black line) solution and a 1 mM FcMeOH + 12 mM β-D-glucose (red line) deareated phosphate buffered (pH 7) aqueous solution. $T = 25$ °C.

the subsequent local pH changes). Finally, by using the B value reported in Table 2 and a diffusion coefficient for FcMeOH of ~$(4-7) \times 10^{-6}$ cm^2 s^{-1},[34−39] the diffusion layer of the redox mediator would result in being ~10^{-3} cm, that is, much thicker than the GOx/11-MUA SAM (~10^{-6} cm), thus confirming that the current response is controlled by the enzymatic reaction rather than by the availability of the redox mediator at the reaction site.[34−39]

An estimate of GOx coverage can now be obtained from the analysis of the steady-state current steps shown in Figure 7. When the diffusion of the enzyme may be neglected, as in the present case, and steady-state conditions are assumed for the enzyme reaction, the rate of the latter process is given by eq 10[34]

$$\frac{i_{cat}}{2FA} = \upsilon = \frac{k_2\Gamma_E}{(K_S/C_S) + (K_M/C_O) + 1} \quad (10)$$

where Γ_E is the surface coverage of GOx, C_S and C_O are the bulk concentrations of substrate (glucose) and redox mediator, respectively, and the other symbols are defined in Scheme 3. From the slope of the Lineweaver−Burk plot, where the reciprocal of the catalytic current values displayed in Figure 7 is plotted versus C_S^{-1} (inset of Figure 7), and assuming $k_2/K_S \approx 11$ mM^{-1} s^{-1} (value obtained by averaging the values reported for FcMeOH in refs 34−39, that are virtually independent of

enzyme and redox mediator concentration), Γ_E was then estimated to be about 1.2×10^{-12} mol cm^{-2}. Such a coverage, that is significantly lower than the maximum coverage of glucose oxidase on solid electrodes (2.9×10^{-12} mol/cm^2),[51] is however in agreement with the recently reported value of 1.16×10^{-12} mol cm^{-2} determined by scanning tunneling microscopy (STM).[46] The above value might in fact represent an underestimate of coverage due to the random orientation of protein molecules onto the SAM surface that is likely to affect their effective electrical wiring.[34−39]

Conclusions

The mechanism of electron transfer through densely packed and well-ordered SAMs of 11-mercaptoundecanoic acid on gold, either pristine or modified by physically adsorbed glucose oxidase, was investigated quantitatively by cyclic voltammetry and electrochemical impedance spectroscopy. The results confirmed that, in the presence of ferrocenylmethanol as a redox mediator, electron transfer kinetics involving either solution-phase species such as $[Fe(CN)_6]^{3-/4-}$ or surface-immobilized GOx does occur primarily according to the so-called *membrane model* that comprises permeation to some extent of the redox mediator within the SAM followed by the intermolecular ET to the redox probe located outside the monolayer. By using digital simulation techniques, kinetic and thermodynamic parameters relevant to the above mechanism were obtained from the CV and EIS data, also providing structural information about the SAM. The validity of the above model was also assessed in the case of the enzymatic electrochemical conversion of glucose to gluconolactone promoted by FeMeOH at the GOx/SAM electrode. EIS measurements highlighted subtle effects on the kinetics of mediated ET associated with the presence (and activity) of the protein, and the analysis of the catalytic current allowed the high surface protein coverage suggested by X-ray photoelectron spectroscopy measurements to be confirmed.

Acknowledgment. This work received support from the PAI P5/01, the Italian MIUR, the University of Bologna, and the FOM (The Netherlands). This research was supported in part also by the Rijksuniversiteit Groningen's Breedtestrategie program.

References and Notes

(1) Finklea, H. O. In *Electroanalytical Chemistry*; Bard A. J., Rubinstein I., Eds.; Marcel Dekker: New York, 1996; Vol. 19, pp 109−135.
(2) Clegg, R. S.; Hutchison, J. E. In *Electron Transfer in Chemistry*; Balzani, V., Ed.; Wiley-VCH: Weinheim, Germany, 2001; Vol. 4, pp 541−557.
(3) Tran, E.; Rampi, M. A.; Whitesides, G. M. *Angew. Chem., Int. Ed.* **2004**, *43*, 3835.
(4) Cecchet, F.; Rudolf, P.; Rapino, S.; Margotti, M.; Paolucci, F.; Beggerman, J.; Brouwer, A. M.; Kay, E. R.; Wong, J.; Leigh, D. A. *J. Phys. Chem. B* **2004**, *108*, 15192.
(5) Porter, M. D.; Bright, T. B.; Allara, D. L.; Chidsey, C. E. D. *J. Am. Chem. Soc.* **1987**, *109*, 3559.
(6) Lenk, T. J.; Hallmark, V. M.; Hoffmann, C. L.; Rabolt, J. F.; Castner, D. G.; Erdelen, C.; Ringsdorf, H. *Langmuir* **1994**, *10*, 4610.
(7) Tam-Chang, S.-W.; Biebuyck, H. A.; Whitesides, G. M.; Jeon, N.; Nuzzo, R. A. *Langmuir* **1995**, *11*, 4371.
(8) Slowinski, K.; Chamberlain, R. V.; Miller, C. *J. Am. Chem. Soc.* **1997**, *119*, 11910.
(9) Chidsey, C. E. D. *Science* **1991**, *251*, 919.
(10) Adams, D. M.; Brus, L.; Chidsey, C. E. D.; Creager, S.; Creutz, A.; Kagan, C. R.; Kamat, P. V.; Lieberman, R.; Lindsay, S.; Marcus, R. A.; Metzger, R. M.; Michel-Beyerle, M. E.; Miller, J. R.; Newton, M. D.; Rolison, D. R.; Sankey, O.; Schanze, K. S.; Yardley, J.; Zhu, X. *J. Phys. Chem. B* **2003**, *107*, 6668.
(11) Liu, B.; Bard, A. J.; Mirkin, M. V.; Creager, S. E. *J. Am. Chem. Soc.* **2004**, *126*, 1485.
(12) Paddon-Row, M. N. In *Stimulating Concepts in Chemistry*; Vogtle, F., Stoddart, J. F., Shibasaki, M., Eds.; Wiley-VCH: Weinheim, Germany, 2000; pp 267−292.
(13) Katz, E.; Shipway, A. N.; Willner, I. In *Electron Transfer in Chemistry*; Balzani, V., Ed.; Wiley-VCH: Weinheim, Germany, 2001; Vol. 4, pp 127−201.
(14) Niki, K. In *Encyclopedia of Electrochemistry*; Bard, A. J., Stratmann, M., Eds.; Wiley-VCH: Weinheim, Germany, 2002; Vol. 9 (Bioelectrochemistry), pp 341−364.
(15) Fedurco, M. *Coord. Chem. Rev.* **2000**, *209*, 263.
(16) Cannes, C.; Kanoufi, F.; Bard, A. J. *Langmuir* **2002**, *18*, 8134.
(17) Cannes, C.; Kanoufi, F.; Bard, A. J. *J. Electroanal. Chem.* **2003**, *547*, 83.
(18) Campuzano, S.; Gálvez, R.; Pedrero, M.; de Villena, F. J. M.; Pingarrón, J. M. *J. Electroanal. Chem.* **2002**, *526*, 92.
(19) Amatore, C.; Saveant, J.-M.; Tessier D. *J. Electroanal. Chem.* **1983**, *147*, 39.
(20) Cecchet, F.; Pilling, M.; Hevesi, L.; Schergna, S.; Wong, J. K. Y.; Clarkson, G. J.; Leigh, D. A.; Rudolf, P. *J. Phys. Chem. B* **2003**, *107*, 10863.
(21) Duwez, A.-S. *J. Electron Spectrosc. Relat. Phenom.* **2004**, *134*, 97.
(22) Schreiber, F. *Prog. Surf. Sci.* **2000**, *65*, 151.
(23) Flink, S.; van Veggel, F. C. J. M.; Reinhoudt, D. N. *Adv. Mater.* **2000**, *12*, 1315.
(24) Diao, P.; Jiang, D.; Cui, X.; Gu, D.; Tong, R.; Zhong, B. *J. Electroanal. Chem.* **1999**, *464*, 61.
(25) Terrettaz, S.; Becka, A. M.; Miller, C. *J. Phys. Chem.* **1995**, *99*, 11216.
(26) Bard, A. J.; Faulkner, L. R. *Electrochemical Methods*; Wiley: New York, 2001.
(27) Boukamp, B. A. *Solid State Ionics* **1986**, *20*, 31.
(28) Bisquert, J.; Garcia-Belmonte, G.; Fabregat-Santiago, F.; Compte, A. *Electrochem. Commun.* **1999**, *1*, 429.
(29) Zoltowski, P. *J. Electroanal. Chem.* **1998**, *443*, 149.
(30) Láng, G.; Heusler, K. E. *J. Electroanal. Chem.* **1998**, *457*, 257.
(31) Sadkowski, A. *J. Electroanal. Chem.* **2000**, *481*, 222.
(32) Fawcett, W. R.; Fedurco, M.; Kovacova, Z. *Langmuir* **1994**, *10*, 2403.
(33) Takehara, K.; Takemura, H.; Ide, Y. *Electrochim. Acta* **1994**, *39*, 817.
(34) Yokoyama, K.; Kayanuma, Y. *Anal. Chem.* **1998**, *70*, 3368.
(35) Hodak, J.; Etchenique, R.; Calvo, E. J.; Singhal, K.; Bartlett, P. N. *Langmuir* **1997**, *13*, 2708.
(36) Bourdillon, C.; Demaille, C.; Moiroux, J.; Savéant, J.-M. *J. Am. Chem. Soc.* **1993**, *115*, 2.
(37) Bourdillon, C.; Demaille, C.; Moiroux, J.; Savéant, J.-M. *J. Am. Chem. Soc.* **1994**, *116*, 10328−10329.
(38) Bourdillon, C.; Demaille, C.; Moiroux, J.; Savéant, J.-M. *Acc. Chem. Res.* **1996**, *29*, 529.
(39) Anicet, N.; Bourdillon, C.; Moiroux, J.; Savéant, J.-M. *J. Phys. Chem. B* **1998**, *102*, 9844.
(40) Pierrat, O.; Lechat, N.; Bourdillon, C.; Laval, J.-M. *Langmuir* **1997**, *13*, 4112.
(41) Khoshtariya, D. E.; Dolidze, T. D.; Zusman, L. D.; Waldeck, D. H. *J. Phys. Chem. A* **2001**, *105*, 1818.
(42) French, M.; Creager, S. E. *Langmuir* **1998**, *14*, 2129.
(43) Bard, A. J.; Faulkner, L. R. *Electrochemical Methods*; Wiley: New York, 2001; pp 380−381.
(44) Katz, E.; Willner, I. *Electroanalysis* **2003**, *15*, 913.
(45) Mirsky, V. M. *Trends Anal. Chem.* **2002**, *21*, 439.
(46) Losic, D.; Shapter, J. G.; Gooding, J. J. *Langmuir* **2002**, *18*, 5422.
(47) Azzaroni, O.; Vela, M. E.; Martin, H.; Creus, A. H.; Andreasen, G.; Salvarezza, R. C. *Langmuir* **2001**, *17*, 6647.
(48) Molinero, V.; Calvo, E. J. *J. Electroanal. Chem.* **1998**, *445*, 17.
(49) Denis, F. A.; Hanarp, P.; Sutherland, D. S.; Gold, J.; Mustin, Ch.; Rouxhet, P.; Dufrêne, Y. F. *Langmuir* **2002**, *18*, 819.
(50) Beamson, G.; Briggs, D. *High Resolution XPS of Organic Polymers−The Scienta ESCA Database*; Wiley: Chichester, U.K., 1992.
(51) Hecht, H. J.; Schomberg, D.; Kalisz, H.; Schmid, R. D. *Biosens. Bioelectron.* **1993**, *8*, 197.
(52) Sluyters-Rehbach, M.; Sluyters-Rehbach, J. H. In *Electroanalytical Chemistry*; Bard, A. J., Ed.; Marcel Dekker: New York, 1970; Vol. 4.
(53) Deslouis, C.; Tribollet, B. *Electrochim. Acta* **1978**, *23*, 935.